Original Research Article

Structural Characterization, DFT, Molecular Docking and Cytotoxic Studies of Metal (II) Complexes Derived from Thiosemicarbazide

ABSTRACT

Co(II), Ni(II) and Cu(II) complexes of N and O donor ligand derived from ,5-dinitrosalicylicacid and thiosemicarbazide, the spectroscopy techniques like UV-Visible, FT-IR, NMR, mass spectrometry, p-XRD and SEM analysis were used to structurally characterize the metal complexes. From the analytical and spectral evidence, the square planar and octahedral geometry has been proposed to metal (II) complexes. In addition to this computational density functional theory (DFT) using B3LYP/6-31Gþ(d, p)/Lanl2dz(f) method in the ground state was performed, the calculations were done to confirm the geometry of the complexes and also HOMO-LUMO excitation energies levels were also calculated. Additionally, MTT test was used to perform cytotoxic assays on selected MCF-7 (estrogen receptor-positive human breast cancer cells) and HeLa (human cervical cancer cell line) cell lines. The antibacterial test was performed via the disc plate method against Escherichia coli and Staphylococcus aureus, and was further supported by molecular docking interactions using protein receptor SEC2 (PDB code: 1STE) in Staphylococcus aureus.

Keywords: Metal complexes, DFT, XRD, SEM, Cytotoxicity, Molecular docking

1. INTRODUCTION

Metal complexes have remained one of the most prominent stereo-chemical models in main group and transition metal coordination chemistry due to their preparative accessibility, diversity, and structural variability [1]. Inorganic medications are made with metal-based and metal-binding substances. Inorganic compounds have long been used in medicine, and their relevance has been recognized. [2-3]. The strong aromaticity of this ring structure leads to exceptional in vivo stability and lack of toxicity in higher vertebrates, including humans, and derivatives of 1,3,4-thiadiazole have significant biological activity. When this ring is connected to a variety of functional groups that interact with biological receptors, compounds with unique properties develop [4]. The 5-amino-l,3,4-thiadiazole-derivatives are the most significant examples, with the exception of several antibacterial sulfonamides (albucid and globucid), which are no longer used clinically but have historical relevance [5-6]. Keeping in view the prior literature, the current study discusses the synthesis, structural elucidation, and morphological analyses of novel metal (II) complexes derived from 3,5-dinitrosalicylicacid and thiosemicarbazide, as well as biological and molecular docking studies.

2. EXPERIMENTAL PART

2.1 Reagents and physical measurements

All the chemicals used were of analytical grade and were as procured. The reagent grade chemicals 3,5-dinitrosalicylicacid, thiosemicarbazide, phosphorous oxychloride and metal (II) salts were purchased from Sigma-Aldrich chemical Co, and used without further purification. 1H-NMR spectra were recorded on a Bruker400MHz spectrometer at IISc, Bangalore, and Karnataka, INDIA. Melting points were recorded using an electro-thermal melting factor equipment and are uncorrected. With tetramethylsilane (TMS) as an internal standard, the chemical shifts have been demonstrated in d values (ppm). Shimadzu, LCMS 2010A, Japan, collected LC-MS with the use of a C-18 column. The compounds' FT-IR spectra were collected as KBr pellets (100mg) using a Shimadzu FT-IR spectrometer. At 35°C, magnetic susceptibility was measured using the Gouy balance model 7550 with Hg[Co(NCS)4] as the calibrant. The compounds' X-ray diffraction analyses were performed on a Bruker AXS D8 prior instrument. A Ziess scanning electron microscope was used to examine the surface morphology of the produced compounds.

2.2 Synthesis of ligand (TS)

The mixture of 3,5-dinitrosalicylicacid (0.02 mol), thiosemicarbazide (0.02 mol), and phosphorous oxychloride (10ml) was heated for 4-5 hours at reflux. After cooling, the mixture was added to 50 mL of distilled water and heated under reflux for another 4 hours. To neutralize the filtrate, potassium hydroxide was utilized. After that, the precipitate was filtered and washed in cold distilled water before being recrystallized with an ethanol-water solvent mixture to get ligand 2-(5-amino-1,3,4-thiadiazol-2-yl)-4,6-dinitrophenol (TS). Molecular formula $C_8H_5N_5SO_5$, Molecular weight 283.22, Brownish yellow solid, Melting point 265^{o}C, Anal.Calcd [%]: C[33.93], H[1.78], N[24.73]; Found[%]: C[34.33], H[1.38], N[25.13].

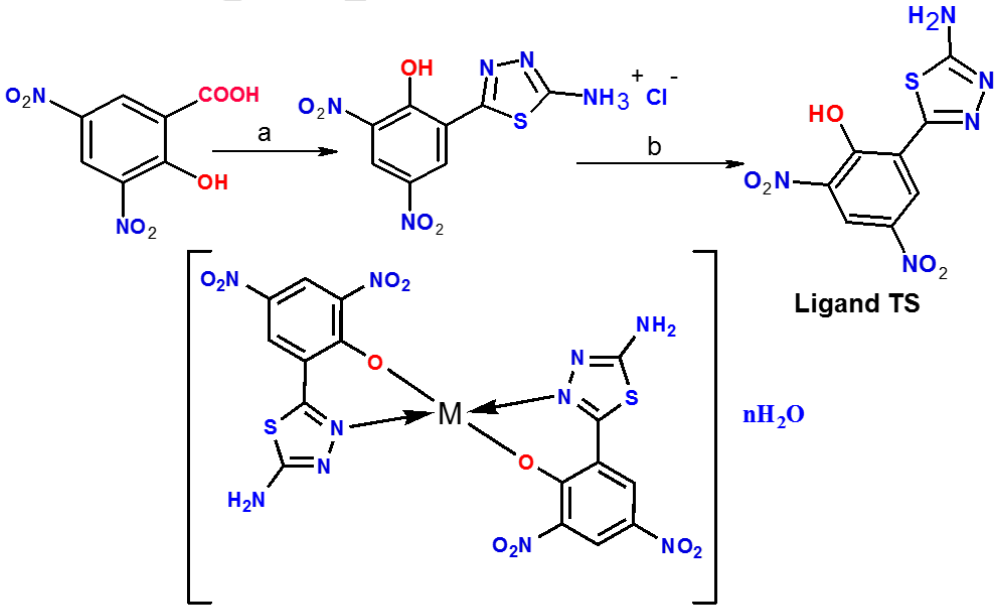

M = Co(II), Cu(II) and Ni(II)

Scheme 1. Synthesis route a) Thiosemicarbazide, $POCl_3$, reflux 4-5hrs, b) KOH

2.3 Preparation of metal (II) complexes

As a general method, the required weight of the free ligand TS is used. The metal chlorides were dissolved in 20 mL methanol and then slowly added to the ligand solution while magnetic stirring was done. After filtering out the precipitates, they were washed in hot methanol and dried at 600 °C for about an hour.

Cu(II) complex [1]

Molecular formula [$C_{16}H_{10}Cl_2CuN_{10}O_{10}S_2$], molecular weight 698.88, Greenish solid; Anal. Calcd [%] :C[28.24], H[1.51] N[20.94]; Found[%]: C[28.64], H[0.98], N[21.34]; Melting point > 300, Molar conductance (λm cm^2 Ω^{-1} mol^{-1}): 23.

Ni (II) complex [2]

Molecular formula [$C_{16}H_{10}Cl_2NiN_{10}O_{10}S_2$], molecular weight 694.02, Greenish solid; Anal. Calcd [%]: C[28.24], H[1.51], N[20.94]; Found[%] :C[28.64] , H[0.98], N[21.34], Melting point > 300, Molar conductance (λm cm^2 Ω^{-1} mol^{-1}): 19.

Co(II) complex [3]

Molecular formula [$C_{16}H_{10}Cl_2CoN_{10}O_{10}S_2$], bluish gray solid, molecular weight 694.26; Anal. Calcd [%]: C[28.74], H[1.51], N[21.94]; Found [%] :C[29.14], H[1.11], N[21.34], Melting point >300, Molar conductance (λm cm^2 Ω^{-1} mol^{-1}): 21.

3. DFT STUDIES

The Gaussian 09 software programme was used to perform all density functional theory (DFT) calculations for the ligand TS and its metal (II) complexes [7-8]. The geometrical structure of the ground state was obtained using Backe's three parameter hybrid exchange functional (B3LYP) and the LANL2DZ basic set in gas phase [28]. For the investigated molecules, the time dependent DFT technique (TD-DFT) was utilised to characterise excited states and electronic transitions based on their optimum ground state geometry, equilibrium geometric parameters, and quantum chemical features such as MEP and HOMO-LUMO energy gap (ΔE).

4. BIOLOGICAL STUDIES

4.1 Antibacterial activity

The antibacterial activity of Escherichia coli and Staphylococcus aureus was evaluated using the paper disc plate method [9]. Each chemical was dissolved in DMSO and concentration solutions (10 g / mL) were produced separately. Paper discs of uniform diameter (2 cm) of Whatman filter paper (No. 42) were cut and sterilised in an autoclave. After being soaked in the required concentration of the complex solutions, the paper discs were placed aseptically on petri plates containing nutritious agar media (agar 20 g + beef extract 3 g + peptone 5 g) seeded with E. coli and S. aureus bacteria separately. The inhibitory zones were determined after the petri dishes were incubated at 37°C for 24 hours. The antibacterial activity of tetracyclin, a common standard antibiotic [10], was also determined using the

same method and solvent as before. The formula for calculating the percent Activity Index for the complex is as follows:

***% Activity Index** = = zone of inhibition by test compound (diameter) / zone of inhibition by standard (diameter) ×100

4.2 Cytotoxicity activity

In vitro antitumor activity was evaluated using the MTT assay [11]. Cells were cultured in 96 well tissue culture plates at a concentration of 1x104 cells/well and incubated overnight at 37 °C in 5% CO2 in a humid air condition to allow for growth and attachment. After that, the cells were cultured in various doses of complexes dissolved in DMSO for 24 hours (1-100g mL-1). After incubation, the culture was removed and each well was filled with 20 µL MTT solution. The plates were then incubated for 4 hours in a CO_2 atmosphere at 37 °C in the dark at 570 nm, the absorbance of the wells was measured using an ELISA reader. The % of cell inhibition expressed as Inhibition (%) = 1 – 100 × (OD toxicant) / (OD –ve control). IC_{50} . The nonlinear regression programme was used to analyze the values.

4.3 Molecular Docking Studies

The bacterial strain used in this docking experiment was selected. In the field of molecular modelling, docking is a technique for predicting ligand conformational and orientation in the binding pocket of a receptor [12-13]. Using the HEX 8.0 programme and the discovery studio visualizer tools, the compounds are docked in the active sites of protein receptors. The Staphylococcus aureus, the protein receptor SEC2 (PDB code: 1STE) was obtained from the Protein Data Bank (http://www.rcsb.org/pdb).

5 RESULTS AND DISCUSSION

According to the results of the elemental analysis and several physical properties of the generated compounds, the Metal (II) Complexes are air-stable, hygroscopic, possess higher melting temperatures, are insoluble in H_2O and most organic solvents, but soluble in DMSO and DMF.

5.1 FT-IR spectral studies

The FT-IR data reveal the ligand's binding modes to metal ions, as reported in Table 1. Infrared spectra were acquired in the region 4000-400 cm^{-1}. The absorption bands at 3415, 1692, 1338, and 1260 cm^{-1} in the IR spectra of free ligand are attributed to the υ(OH), υ(C=N), υ(C-N) and υ(C-O) stretching modes, respectively[14].

The disappearance of -OH bands in the spectra of metal (II) complexes implies deprotonation of the intramolecular hydrogen bond OH group during complexation and subsequent coordination of phenolic oxygen to the metal ion, which is supported by the shift of υ(C-O) (phenolic) by 10-15 cm^{-1}. When compared to the free ligand, the (C=N) band shifted to lower wave numbers, indicating that the azomethine group's nitrogen was coupled to the metal ion. The (C-N) band is further supported by a lower shift of 25-30 cm^{-1}. Similarly, the presence of two new non-ligand medium intensity bands in the 440-442 cm^{-1} and 477-485 cm^{-1} bandwidths, which have been attributed to the M-N and M-O bands, respectively

[15], is related to the coordination of metal ions. According to the IR data of the ligand TS and its metal complexes, metal (II) complexes in nature behave as bidentate. The IR spectrum are given in the supplementary file S1 to S4.

Table 1. FT-IR spectral bands of ligand and its metal (II) complexes

Compounds	-OH	-NH	-C=N	-C-N	-C-O	-CH Str	M-O	M-N
TS	3415	3269	1692	1338	1260	2900	-	-
Co(II)TS_2	-	3250	1672	1309	1256	2786	485	440
Ni(II)TS_2	-	3250	1657	1306	1254	3088	477	441
Cu(II)TS_2	-	3252	1653	1310	1248	3010	471	445

5.2 UV-visible spectral studies

All of the compounds' electronic absorption spectra were measured at room temperature using DMF solution in the range of 200-900nm [16]. The spectral measurements of the uncoordinated ligand revealed two different absorption regions and are shown in Table 2. The aromatic rings of the π-π* transition are responsible for the absorption band at 287 nm (34,843cm^{-1}), whereas the n-π* electronic transition is responsible for the absorption band at 349 nm (28,653cm^{-1}). The electronic spectrum are given in supplementary file S4 [28-33]. Table 2 shows the electronic spectrum and magnetic data of metal (II) complexes. Cu(II) complexes have two electronic absorption bands about 17,813, 26525 cm^{-1}, which are assigned to $^2B_{1g} \rightarrow {}^2A_{1g}$ and intra-ligand charge transfer bands, respectively [17], implying a square planar geometry and a magnetic value of 1.72 BM.

The Co(II) complex has two absorption bands at 17,857 and 16,393 cm-1, corresponding to electronic transitions $^4T_{1g}$ (F)→$^4T_{1g}$, (P) and $^4T_{1g}$ (F)→$^4T_{2g}$, (F), implying octahedral geometry, and the measured magnetic susceptibility value of 4.67 BM is significantly related to higher spin octahedral arrangement [18]. The absorption bands of Ni(II) complex exhibit two bands at 15,384. 14,985 cm^{-1} that are assigned to $^3A_{2g}$ (F)→$^3T_{1g}$, (P) and $^3A_{2g}$ (F)→$^3T_{1g}$, (P) transitions, respectively. The magnetic moment value of 3.12 BM obtained from these transitions indicates a high spin octahedral geometry for Ni(II) complex.

Table 2. Electronic spectral data of metal complexes

Compounds	Absorption bands (cm^{-1})	Transition	Geometry	μ_{eff} (BM)
Co(II)TS_2	17,857, 16,393	$^4T_{1g}$ (F)→$^4T_{1g}$, (P) $^4T_{1g}$ (F)→$^4T_{2g}$, (F)	Octahedral	4.67
Ni(II)TS_2	15,384. 14,985	$^3A_{2g}$ (F)→$^3T_{1g}$, (P) $^3A_{2g}$ (F)→$^3T_{1g}$, (P)	Octahedral	3.12
Cu(II)TS_2	17,813, 26525	$^2B_{1g} \rightarrow {}^2A_{1g}$, INCT	Square planar	1.72

5.3 ^{1}H-NMR and Mass spectral studies

The ^{1}H NMR spectra of the ligand TS in DMSO d6 at room temperature were obtained using TMS as an internal standard. The TS exhibited a sharp peak for d(OH) protons at 10.36 ppm, 5.56 ppm for

d(NH2) protons at 5.56 ppm, and aromatic protons from 7.77 to 7.73 ppm, respectively. The mass spectrum of the ligand (TS) was recorded, and the observed molecular ion peak confirms the proposed formulae. The mass spectrum of the ligand (TS) shows a well-defined molecular ion peak at m/z 284.9 (283.2), which corresponds to the molecular formula weight (M+1).^{1}H NMR and mass spectrum are given supplementary file S5 and S6.

5.4 SEM studies

The scanning electron microscope (SEM) was used to depict the surface morphology and grain size of metal complexes [19]; SEM micrographs are presented in Figure 1**,** and the particles are agglomerated in a controlled morphological structure, with small grains of non-uniform size remaining. With a particle size of 10 m, the ligand TS exhibited an irregular ice grain-like shape. The Co(II) and Ni(II) complexes, on the other hand, have an ice rock-like shape with particle sizes of 7 and 2 µm, respectively. The Cu(II) complex micrograph exhibits a tiny needle-like morphology with a particle size of 5 µm. The complexation of metal ions with the ligand TS and their metal complex crystal aggregates deposited on the thin films was the key factor that modified the shape of the ligand TS and their metal complex crystal aggregates [20].

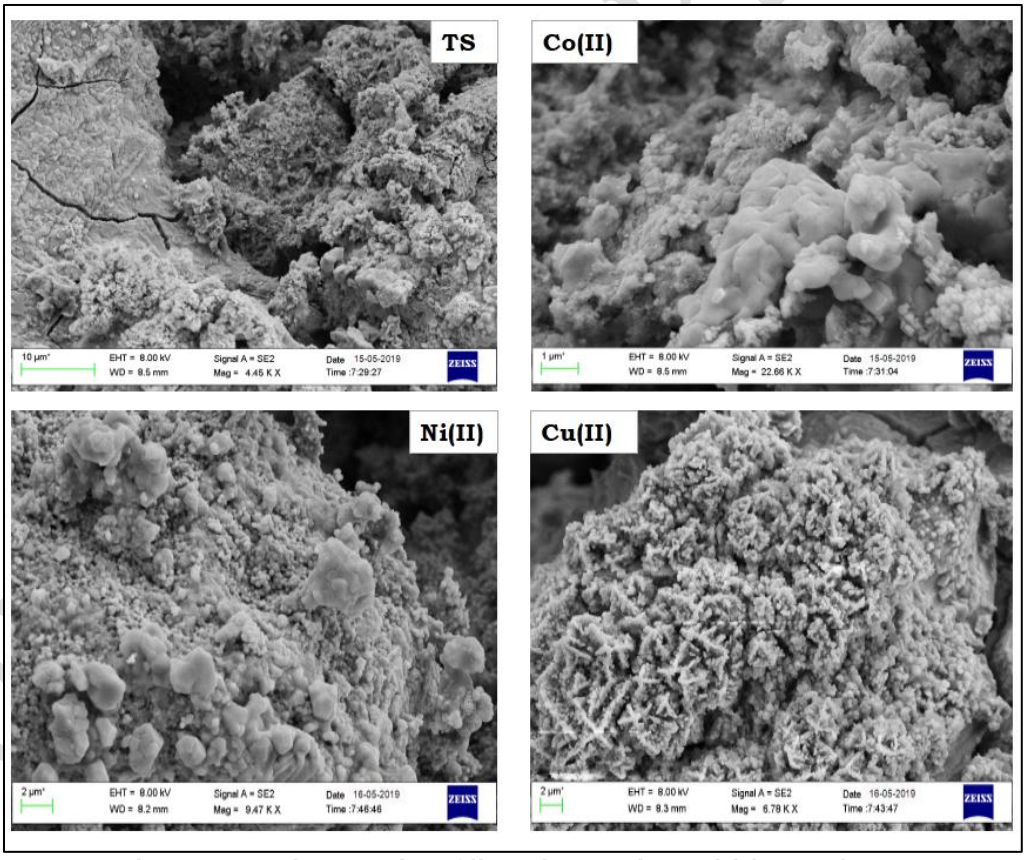

Fig. 1. SEM micrographs of ligand TS and metal (II) complexes

5.5 X-ray diffraction studies

To gain more information concerning the structure of the metal (II) complexes, X-ray diffraction was performed and recorded at 2θ = 10-80°; the diffractograms are presented in Figure 2. The crystalline nature of the Co(II) and Cu(II) metal complexes is indicated by sharp crystalline peaks in the ranges of 6.51 to 30.45° and 8.21 to 25.83°, respectively, and the slight crystalline nature of the Ni(II) complexes in the range of 10.25 to 19.41°. The Miller indices (hkl) are shown in Tables 3 and 4, along with observed and calculated d angles, 2θ values, and relative intensities [21]. The Debye Scherrer equation (D =Kƛ/βCosθ) was used to compute the average crystallite sizes dxrd of the complexes. Where D denotes particle size, K denotes Dimensionless shape factor, and ƛ = X-ray wavelength (0.15406 Å). θ = Diffraction angle, β = Line broadening at half maximum intensity. Co(II), Ni(II), and Cu(II) complexes have average crystallite sizes of 28.44, 37.23, and 27.18 nm, respectively[22].

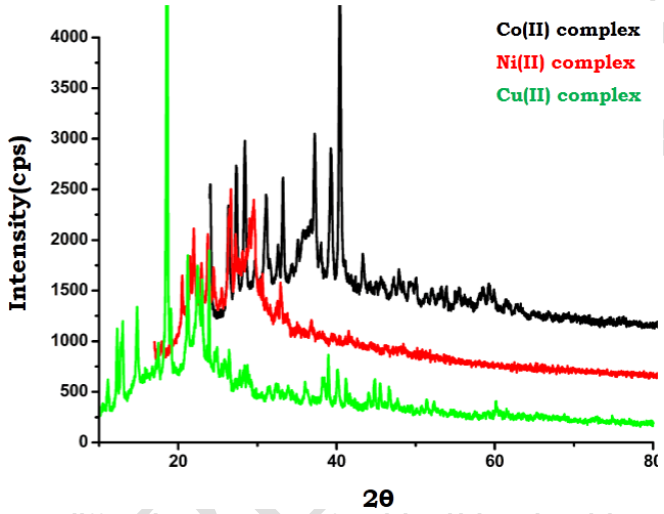

Fig. 2. X-ray diffraction patterns of Co(II), Ni(II) and Cu(II) complexes

Table 3. XRD data of Co(II) complex

Peak No	2θ	θ	Sinθ	h k l	d		Intensity	a in Å
					Cal	obs		
1	12.383	6.191	0.107	1 1 0	11.57	11.568	20.9	6.35
2	13.344	6.672	0.116	1 1 0	10.45	10.443	100	6.35
4	14.425	7.212	0.125	4 2 0	9.088	9.089	51.9	6.35
5	15.709	7.854	0.136	4 0 4	6.512	6.512	37.7	6.35
6	17.150	8.575	0.149	6 6 1	4.203	4.202	16.8	6.35
7	17.601	8.801	0.153	6 2 7	4.054	4.054	20.4	6.35
8	18.619	9.310	0.161	6 1 4	5.211	5.21	20.6	6.35

Table 4. XRD data of Cu(II) complex

Peak No	2θ	θ	Sinθ	h k l	d		Intensity	a in Å
					Cal	obs		
1	10.961	5.480	0.095	1 1 0	10.51	10.52	100	3.62
2	13.501	6.751	0.117	3 8 9	8.396	8.369	57.9	3.62
4	14.501	7.251	0.126	4 1 4	7.825	7.822	71.0	3.62
5	14.942	7.471	0.130	4 5 0	6.89	6.89	70.8	3.62
6	15.922	7.961	0.138	4 2 0	6.63	6.639	56.6	3.62
7	16.759	8.379	0.145	4 4 8	6.02	6.018	52.8	3.62

8	17.460	8.730	0.151	4 3 1	5.57	5.578	57.4	3.62

5.6 DFT Studies

The calculations, optimized geometry, and molecular electrostatic potential (MEP) of Co(II), Ni(II), and Cu(II) complexes are shown in Figures 3, 4, and 5 [23-24]. Molecular electrostatic potential (MEP) is involved with the chemical reactivity and electronegativity of molecules electron and proton. The negative electrostatic potential is represented by the red colour and is mostly found on the NO_2 and nitrogen groups, the blue colour represents the positive electrostatic potential, which is found on the thiadiazole moiety and other molecular skeletons of the molecule. The potential demonstrates that the nucleophilic core of oxygen is nucleophilic, whereas center of nitrogen is electrophilic, resulting in molecular interactions in a complex.

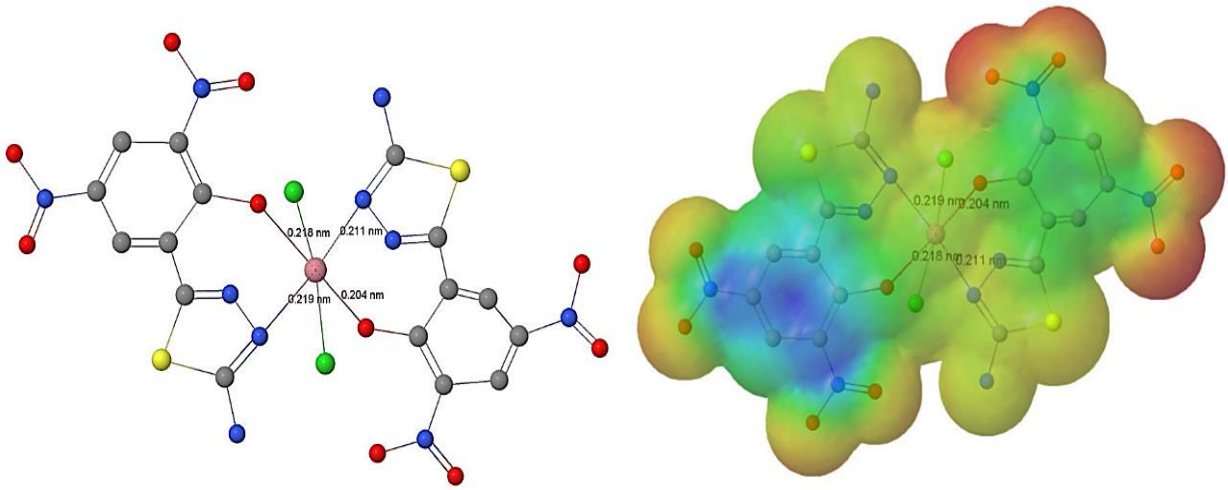

Fig.3. Optimized structure and molecular electrostatic potential (MEP) surface of Co(II) complex

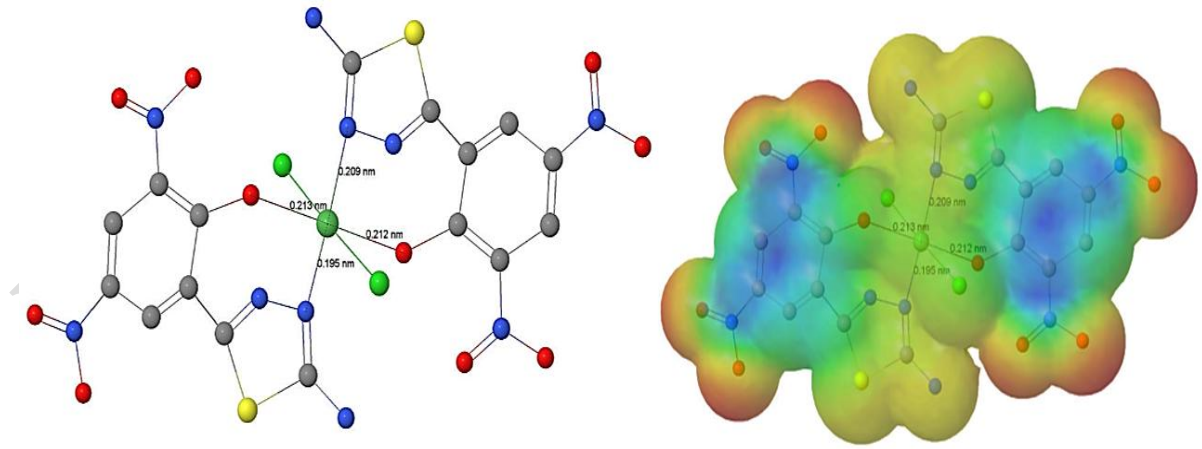

Fig. 4. Optimized structure and molecular electrostatic potential (MEP) surface of Ni(II) complex

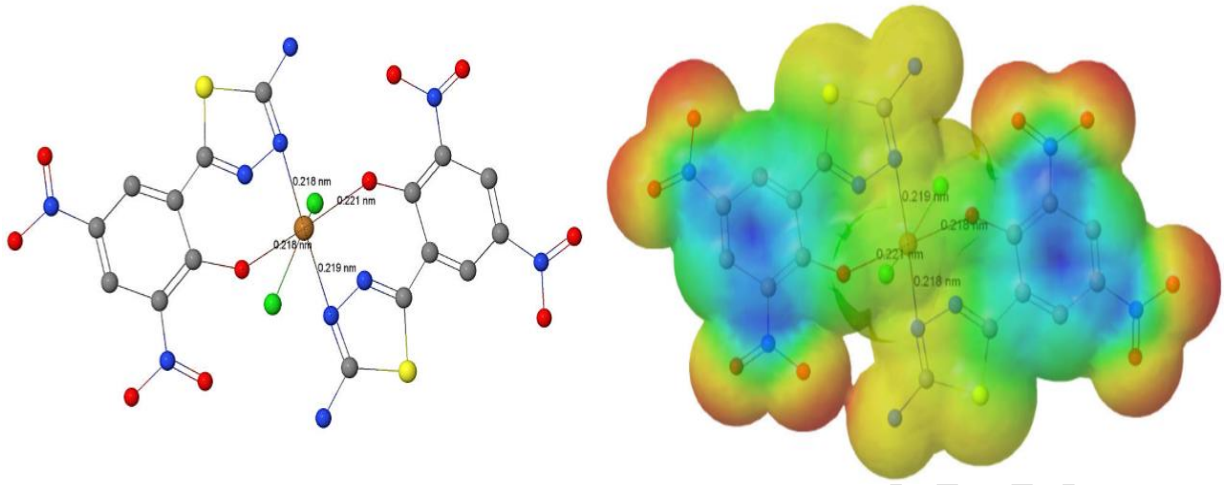

Fig. 5. Optimized structure and molecular electrostatic potential (MEP) surface of Cu(II) complex

Frontier molecular orbital analysis (FMOs)

The molecule's HOMO-LUMO gap is relevant since it relates to specific electron movements and may be extremely significant for single electron transfer. Molecules with a large HOMO-LUMO gap have been discovered to be highly stable and unreactive, whereas those with a small gap are often reactive. The excitation energy and ground state can be easily determined by computing the HOMO-LUMO energy gap. Figure 6 shows the electron density maps of the HOMO and LUMO for the complexes [25]. The electron density is predominantly delocalized on central metal ions and substitution of NO_2, phenolic oxygen group respectively, as can be shown. Electron withdrawing groups like NO_2 produce an increase in the HOMO-LUMO energy and hence a decrease in the energy gap. The HOMO-LUMO energy levels of Co(II), Ni(II), and Cu(II) metal complexes are 1.388eV, 0.468eV, and 4.383eV, respectively. As demonstrated in Tables 5, 6, and 7, these frontier HOMO-LUMO orbital energies are utilized to calculate equilibrium geometric characteristics such as bond lengths, bond angles, and dihedral angles.

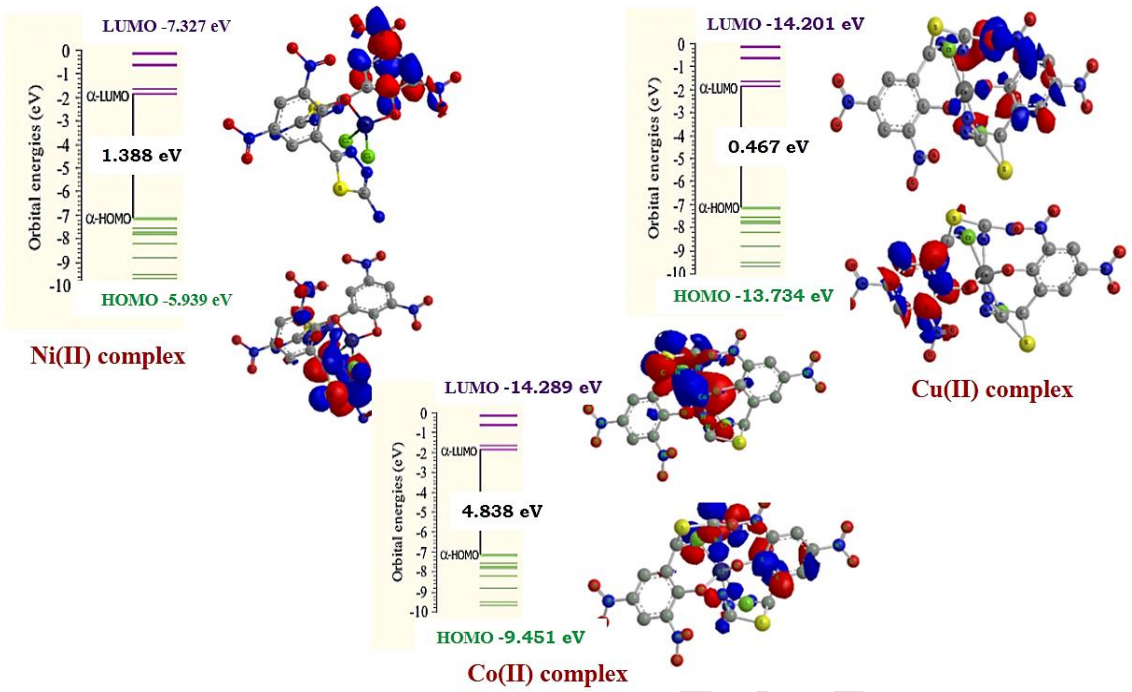

Fig. 6. HOMO-LUMO surfaces of Co(II), Ni(II) and Cu(II) metal complexes simulated by DFT-BL3YP/LANL2DZ level of theory

Table 5. Equilibrium geometric parameters bond lengths, bond angles and dihedral angles of Cu(II) complex

Bond lengths		Bond angles		Dihedral angles	
C(1)-C(2)	1.386	O(20)-Cu(27)	1.81	C(17)-N(39)	1.446
C(1)-C(3)	1.386	N(24)-Cu(27)	1.846	C(18)-C(19)	1.387
C(1)-C(8)	1.54	C(25)-N(26)	1.446	C(18)-N(36)	1.446
C(2)-C(4)	1.386	Cu(27)-Cl(28)	2.16	O(20)-Cu(27)	1.81
C(2)-O(7)	1.41	Cu(27)-Cl(29)	2.16	C(21)-S(22)	1.79
C(3)-C(5)	1.386	C(2)-C(1)-C(3)	120	C(21)-N(23)	1.372
C(4)-C(6)	1.386	C(8)-N(10)-N(11)	119.85	S(22)-C(25)	1.79
C(4)-N(33)	1.446	N(10)-N(11)-C(12)	104	N(23)-N(24)	1.352
C(5)-C(6)	1.386	N(10)-N(11)-Cu(27)	81.299	N(24)-C(25)	1.446
C(5)-N(30)	1.446	C(12)-N(11)-Cu(27)	109.5	N(24)-Cu(27)	1.846
O(7)-Cu(27)	1.81	S(9)-C(12)-N(11)	97.759	C(25)-N(26)	1.446
C(25)-N(26)	1.446	S(22)-C(25)-N(26)	164.72	C(12)-N(11)-Cu(27)	109.5
Cu(27)-Cl(28)	2.16	N(11)-Cu(27)-N(24)	179.43	S(9)-C(12)-N(11)	97.759
Cu(27)-Cl(29)	2.16	O(20)-Cu(27)-N(24)	119.5	S(9)-C(12)-N(13)	169.249
N(30)-O(31)	1.132	N(24)-Cu(27)-Cl(28)	149.43	N(11)-C(12)-N(13)	92.977
N(30)-O(32)	1.316	Cl(28)-Cu(27)-Cl(29)	180	N(23)-N(24)-Cu(27)-Cl(28)	117.508

Table 6. Equilibrium geometric parameters bond lengths, bond angles and dihedral angles of

Co(II) complex

Bond lengths		Bond angles		Dihedral angles	
C(4)-C(6)	1.386	C(4)-C(6)	1.386	N(11)-Co(27)-O(20)	61.063
C(4)-N(33)	1.446	C(4)-N(33)	1.446	N(11)-Co(27)-N(24)	179.427
C(5)-C(6)	1.386	C(5)-C(6)	1.386	N(11)-Co(27)-Cl(29)	150
C(5)-N(30)	1.446	C(5)-N(30)	1.446	O(20)-Co(27)-N(24)	119.499
O(7)-Co(27)	1.8	O(7)-Co(27)	1.8	O(20)-Co(27)-Cl(28)	90.564
C(8)-S(9)	1.79	C(8)-S(9)	1.79	O(20)-Co(27)-Cl(29)	89.436
C(8)-N(10)	1.244	C(8)-N(10)	1.244	N(24)-Co(27)-Cl(28)	149.427
S(9)-C(12)	2.149	S(9)-C(12)	2.149	N(24)-Co(27)-Cl(29)	30.573
N(10)-N(11)	1.094	N(10)-N(11)	1.094	Cl(28)-Co(27)-Cl(29)	180
N(11)-C(12)	1.446	N(11)-C(12)	1.446	C(5)-N(30)-O(31)	120
N(11)-Co(27)	1.836	N(11)-Co(27)	1.836	C(5)-N(30)-O(32)	119.999
C(25)-N(26)	1.446	O(20)-Co(27)-N(24)	119.4	C(25)-N(24)-Co(27)-N(11)	-129.06
Co(27)-Cl(28)	2.15	O(20)-Co(27)-Cl(28)	90.564	C(25)-N(24)-Co(27)-O(20)	39.432
Co(27)-Cl(29)	2.15	O(20)-Co(27)-Cl(29)	89.436	C(25)-N(24)-Co(27)-Cl(28)	-129.06

Table 7. Equilibrium geometric parameters bond lengths, bond angles and dihedral angles of Ni(II) complex

Bond lengths		Bond angles		Dihedral angles	
C(1)-C(2)	1.386	C(5)-C(6)	1.386	C(1)-C(2)	1.386
C(1)-C(3)	1.386	C(5)-N(30)	1.446	C(1)-C(3)	1.386
C(1)-C(8)	1.54	O(7)-Ni(27)	1.79	C(1)-C(8)	1.54
C(2)-C(4)	1.386	C(8)-S(9)	1.79	C(2)-C(4)	1.386
O(7)-Ni(27)	1.79	C(14)-C(15)	1.386	O(7)-Ni(27)	1.79
C(8)-S(9)	1.79	C(14)-C(16)	1.386	C(8)-S(9)	1.79
C(8)-N(10)	1.244	C(14)-C(21)	1.54	C(8)-N(10)	1.244
N(11)-Ni(27)	1.826	C(17)-C(19)	1.386	N(11)-Ni(27)	1.826
C(21)-N(23)	1.455	C(8)-N(10)-N(11)	106.828	N(23)-N(24)	1.352
S(22)-C(25)	1.775	N(10)-N(11)-C(12)	104	N(24)-Ni(27)	1.826
N(23)-N(24)	1.352	N(10)-N(11)-Ni(27)	67.933	C(25)-N(26)	1.446
N(24)-C(25)	1.446	C(12)-N(11)-Ni(27)	109.5	Ni(27)-Cl(28)	2.14
N(24)-Ni(27)	1.826	S(22)-C(25)-N(24)	116.758	Ni(27)-Cl(29)	2.14
Ni(27)-Cl(28)	2.14	S(22)-C(25)-N(26)	164.862	N(30)-O(31)	1.132
Ni(27)-Cl(29)	2.14	N(24)-C(25)-N(26)	78.372	C(25)-N(24)-Ni(27)-Cl(28)	-129.06
N(30)-O(31)	1.132	O(7)-Ni(27)-Cl(29)	90	C(25)-N(24)-Ni(27)-Cl(29)	50.94

6 BIOLOGICAL STUDIES

6.1 Antibacterial activity

The obtained results of antibacterial assay of synthesized compounds have given in the Table 8. The Co(II) and Ni(II) complexes showed significant inhibition of gram positive bacterial strains B. subtilis, S. pneumonia, and S. aureus. Cu(II) complex, on the other hand, exhibited potential efficacy against gram-negative bacteria such as P. aeruginosa and K. pneumonia.. While the ligand TS showed least activity towards all the bacterial strains [26-27].

Table 8. Antibacterial activity of TS and its metal complexes in the form of inhibition zone diameter (mm)

Compounds	Zone of Inhibition (mm)				
	P.aeruginosa	**K. pneumonia**	**B. subtilis**	**S. pneumonia**	**S. aureus**
TS	09	08	07	06	10
$Co(II)TS_2$	14	15	18	12	12
$Ni(II)TS_2$	14	16	19	10	11
$Cu(II)TS_2$	15	18	20	15	15
Ciprofloxacin	**16**	**19**	**22**	**18**	**17**

6.2 *In-silico* molecular docking studies

It is essential to conduct in silico docking studies in relation to antibacterial activity. The Staphylococcus aureus protein receptor SEC2 (PDB: 1STE) showed excellent docking interactions with various amino acids, as well as an E-total score [28]. The Ni(II) complex has a binding affinity of -287.16 kcal/mol for enzyme receptor 1STE, while the Co(II) and Cu(II) complexes had docking scores of -277.42 and -284.32 kcal/mol, respectively. The ligand TS, on the other hand, showed the least binding interactions of -155.73 kcal/mol. The binding of different amino acids such as His6, Phe20, Thr136, Ser165, Phe167, Glu198, Phe200, Val236, Thr237, Leu250, and Leu253 between the ligand and the receptor is shown in Figures 7, 8, and 9.

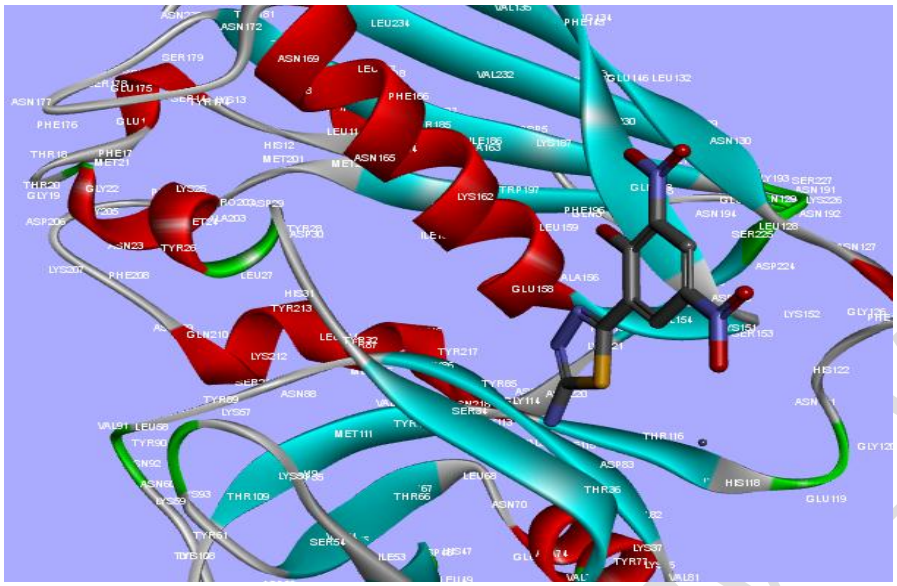

Figure 7. 3D docking interactions of TS with the protein receptor SEC2 (PDB code: 1STE) in Staphylococcus aureus,

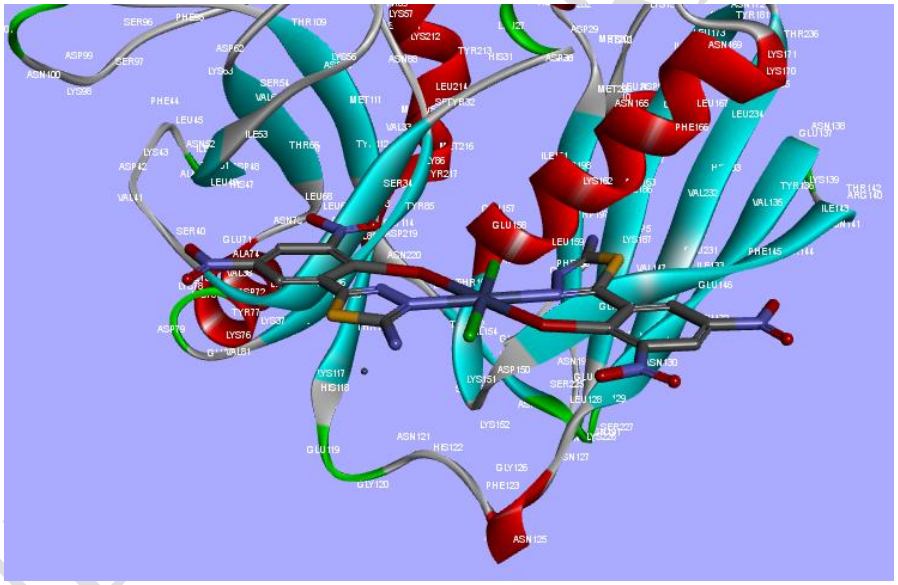

Figure 8. 3D docking interactions of Co(II) complex with the protein receptor SEC2 (PDB code: 1STE) in Staphylococcus aureus,

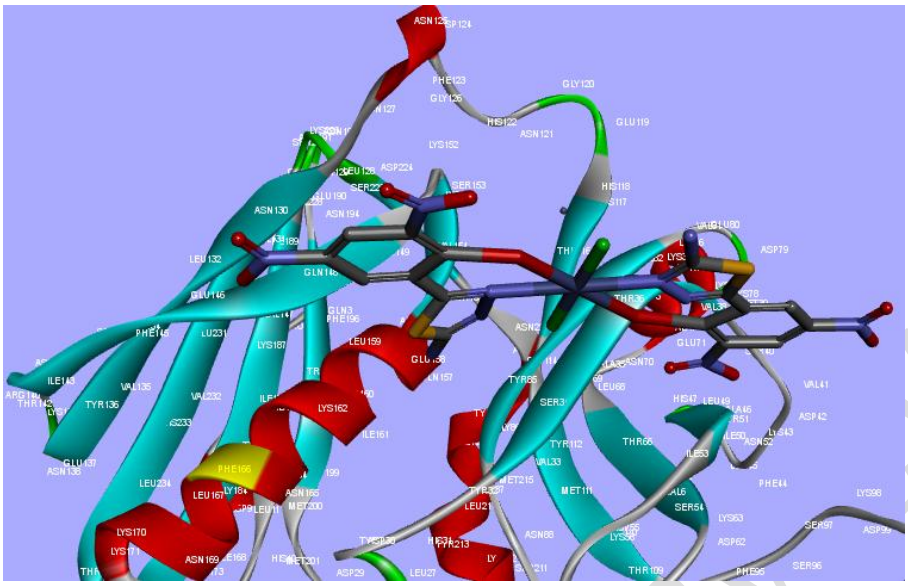

Figure 9. 3D docking interactions of Cu(II) complex with the protein receptor SEC2 (PDB code: 1STE) in Staphylococcus aureus,

6.3 Cytotoxicity assay

On selected MCF-7 (oestrogen receptor-positive human breast cancer cells) and HeLa (human cervical cancer cell line) cell lines, the MTT test was performed to investigate the cytotoxic effect of ligand TS and metal (II) complexes [29-30]. Cisplatin was used as a control drug, and cancer cells were given varying doses of the analyzed samples for 24 hours (1-100 g mL^{-1}). Concentration dependent effects of tested compounds and cell inhibition values against the cancer cells expressed as IC_{50} µg/mL. The obtain results showed that Cu(II) complex exhibits greater cytotoxic effect on MCF-7 (2.852 µg/mL) and HeLa (3.124 µg/mL) cell lines, the ligand TS, Table 9 shows that the Co(II) and Ni(II) complexes had similar moderate values. Cu(II) complex has a more cytotoxic effect due to the strong stacking mode of interaction between the DNA bases of both cancer cell lines [31-32].

Table 9. In vitro cytotoxic studies of (IC_{50} µg/mL) of TS and its complexes against MCF-7, HeLa of human carcinoma cell lines

Compounds	MCF-7	HeLa
TS	12.331	10.412
Co(II)TS_2	6.812	8.861
Ni(II)TS_2	6.955	6.921
Cu(II)TS_2	2.852	3.124
Cisplatin	11.225	13.711

7 CONCLUSION

In this study, synthesis of N, O donar ligand and their metal (II) complexes with Co(II), Ni(II) and Cu(II) ions were prepared and characterized by spectroscopic and analytical methods, the Uv-visble data suggest that Co(II) and Ni(II) complexes octahedral geometry, while on other hand square planar geometry for Cu(II) complexes. XRD and SEM analysis reveal the metal (II) complexes shows well-defined homogenous crystalline nature, DFT studies showed that the metal (II) complexes with slight effect on electron density distribution and FMO's (HOMO-LUMO) energy gap shows significant effect on biological properties. In addition to this cytotoxicity activity with MCF-7 (oestrogen receptor-positive human breast cancer cells) and HeLa (human cervical cancer cell line) cell lines in that Ni(II) complex showed promising inhibition towards both the cell lines. Gram positive bacterial strains B. subtilis, S. pneumonia, and S. aureus were significantly inhibited by the Co(II) and Ni(II) complexes. The Cu(II) complex, on the other hand, showed potential against gram-negative bacteria like P. aeruginosa and K. pneumonia. In consideration of this, molecular docking experiments revealed that the Ni(II) complex had -287.16 kcal/mol binding interactions with various amino acids.

COMPETING INTERESTS DISCLAIMER:

Authors have declared that no competing interests exist. The products used for this research are commonly and predominantly use products in our area of research and country. There is absolutely no conflict of interest between the authors and producers of the products because we do not intend to use these products as an avenue for any litigation but for the advancement of knowledge. Also, the research was not funded by the producing company rather it was funded by personal efforts of the authors.

8 REFERENCES

1. A.Z. El-Sonbati, G.G. Mohamed, A.A. El-Bindary, W.M.I. Hassan, A.K. Elkholy, J. Mol. Liq. **209**, 625–634 (2015).
2. S.H. Alotaibi, A.S. Radwan, Y.K. Abdel-Monem, M.M. Makhlouf, Spectrochim. Acta A. **205**, 364–375 (2018).

3. N. Chitrapriya, V. Mahalingam, M. Zeller, K. Natarajan, Inorg. Chim. Acta **363**, 3685 (2010).
4. J. Joseph, B.H. Mehta, Russ. J. Coord. Chem. **33**, 124–129 (2007).
5. Fawaz A. Saad, Hoda A. El-Ghamry, M.A. Kassem, Appl. Organomet. Chem. **33**, 4965 (2019).
6. K. Singh, M.S. Barwa, P. Tyagi, Eur. J. Med. Chem. **42**, 394–402 (2007).
7. S. Kathiresan, S. Mugesh, J. Annaraj, M. Murugan, New J. Chem.**41**, 1267 (2017).
8. M.J. Frisch, Gaussian 09, Revision A02 (Gaussian Inc., Wallingford, 2009).
9. A.D. Becke, J. Chem. Phys. **98**, 5648 (1993).
10. M. Pfaller, L. Burmeister, M. Bartlett, M. Rinaldi, J. Clin. Microbiol. **26**, 1437 (1988).
11. X. Qiu, S. Abdel-Meguid, C. Janson, R. Court, M. Smyth, D. Payne, Protein Sci. 8, 2529 (1999).
12. S. Mouilleron, M.A. Badet-Denisot, B. Golinelli-Pimpaneau, J. Mol. Biol. **377(4)**, 1174–1185 (2008).
13. H. Wu, J. Kong, Z. Yang, X. Wang, F. Shi, Y. Zhang, Trans. Met.Chem. **39**, 951–960 (2014).
14. H. Liu, H. Wang, F. Gao, D. Niu, Z. Lu, J. Coord. Chem. **60**, 2671–2678 (2007).
15. W. You, H.-Y. Zhu, W. Huang, B. Hu, Y. Fan, X.-Z. You, Dalton Trans. **39**, 7876–7880 (2010)
16. M.S. Masoud, S.S. Hagagg, Alaa E. Ali, N.M. Nsar, J. Mol. Struct.**1014**, 17–25 (2012).
17. A.Z. Sonbati, G.G. Mohamed, A.A. Bindary, W.M.I. Hassan, M.A. Diab, S.M. Morgan, A.K. Elkholy, J. Mol. Liq. **212**, 487–502 (2015).
18. T. Manjuraj, G. Krishnamurthy, Y.D. Bodke, H.S. Bhojya-Naik, J. Mol. Struct. **1171**, 481-487 (2018).
19. D.N. Sathyanarayana, Electronic Absorption Spectroscopy and Related Technique (University Press (India), Hyderabad, 2001).
20. N. Lotf, I. Sheikhshoaei, S.Y. Ebrahimipour, H. Krautscheid, J. Mol. Struct. **432**, 1149 (2017).
21. W.H. Mahmoud, N.F. Mahmoud, G.G. Mohamed, Appl. Organomet. Chem. **1**, 31 (2017).
22. I. Fleming, Frontier Orbitals and Organic Chemical Reactions (Wiley, New York, 1976).
23. P. Thanikaivelan, V. Subramanian, J.R. Rao, B.U. Nair, Chem.Phys. Lett. **59**, 323 (2000).
24. J. Chen, X. Wang, Y. Shao, J. Zhu, Y. Zhu, Y. Li, Q. Xu, Z.J. Guo, Inorg. Chem. **46**, 3306–3312 (2007).
25. Manjuraj T. Yuvaraj TCM, Jayanna N.D, Sarvajith M S, Materials Today: Proceedings, 2021, https://doi.org/10.1016/j.matpr.2021.10.354.
26. T. Manjuraj, T. C. M. Yuvaraj, N.D. Jayanna, S.H. Shreedhara, M.S. Sarvajith, J. Turk. Chem. Socty. Chem-A. **7(2)**, 449-462, (2020).
27. N. Dharmaraj, P. Viswanathamurthi, K. Nataraj, Trans. Met. Chem. **26**, 105–109 (2001).
28. R. Ramesh, S. Maheswaran, J. Inorg. Biochem**. 9**, 457–462 (2003).
29. T. Manjuraj, G. Krishnamurthy, Y.D. Bodke, H.S. Bhojya-Naik, J. Mol. Struct. **1148**, 231–237 (2017).
30. M.A. Gyamf, M. Yonamine, Y. Aniya, Gen. Pharmacol. **32**, 661–667 (1999).
31. B. Koohshekan, A. Divsalar, M. Saiedifar, A.A. Saboury, B. Ghalandari, A. Gholamian, A. Seyedarabi, J. Mol. Liq. **216**, 8–15 (2016).
32. T. Manjuraj, G. Krishnamurthy, Y.D. Bodke, H.S. Bhojya-Naik, Asian J. Research Chem. **10(4),** 470-476, (2017).